Composites Science and Technology 72 (2012) 1283–1290

Contents lists available at SciVerse ScienceDirect

Composites Science and Technology

journal homepage: www.elsevier.com/locate/compscitech

Diametral compression of pultruded composite rods

N.K. Kar *, Y. Hu, B. Ahn [1], S.R. Nutt

Gill Composites Center, Department of Chemical Engineering and Materials Science, University of Southern California, Los Angeles, CA 90089, USA

ARTICLE INFO

Article history:
Received 27 January 2012
Received in revised form 12 April 2012
Accepted 2 May 2012
Available online 11 May 2012

Keywords:
A. Carbon fibers
A. Glass fibers
B. Mechanical properties
D. Acoustic emission

ABSTRACT

Diametral compression tests were performed on pultruded composite rods comprised of unidirectional glass or carbon fibers in a common matrix. During compression tests, acoustic emission (AE) activity was recorded and images were acquired from the sample for analysis by digital image correlation (DIC). In both composite systems, localized tensile strain developed in the transverse plane under the load platens prior to failure, producing non-linearity in the load–displacement curve and AE signals. *In situ* SEM diametral compression tests revealed the development of matrix microcracking and debonding in regions of localized strain, perpendicular to the tensile strain direction (parallel to the load axis). Comparison of linear finite element simulations and experimental results showed a deviation from linear elastic behavior in the load displacement curve. The apparent transverse modulus, in plane shear modulus, and transverse tensile strength of the GF rod was greater than that of the CF rod, and fracture surfaces indicated greater fiber/matrix adhesion in the GF system compared to the CF system. A mixed mode fracture surface showed that two failure modes were active – matrix tensile failure and matrix compression failure by shear near the loading edge.

1. Introduction

High-voltage composite reinforced conductors (CRCs) generally consist of Al wires (to carry current) wrapped around a hybrid composite rod (to provide mechanical support) comprised of a glass fiber (GF) shell and a carbon fiber (CF) core [1–5]. The advent of CRCs has led to investigations to determine the effect of intense mechanical loads, thermal and moisture exposures on such hybrid composite rods. Overhead conductors (power cables) must retain load-bearing capability for several decades with little or no maintenance. As a result, studies have focused on retention of mechanical properties, particularly longitudinal strength, under aggressive environmental conditions and loads [2,3]. Progress has been made to better understand factors affecting the durability of CRCs, although several fundamental issues have not yet been addressed. One such issue concerns the effects of stress concentrations and the associated development of localized strains and modes of failure under complex loading conditions. For example, mechanical collets are used to attach the composite rods at lattice tower nodes, and these fixtures achieve traction by applying transverse loads on the rod surface. Recent studies have shown that transverse loads on the composite core can increase longitudinal stresses and promote fatigue crack propagation under cyclic tensile loads [5]. However, the effect of transverse loads on the in-plane behavior of pultruded composite rods is not yet fully understood.

Because of the cylindrical geometry and the intermingling of carbon and glass fibers in the core/shell design of the hybrid composite rod, accurate measurement of transverse properties poses difficulties, and conventional composite laminate test methods cannot be used. Thus, alternative techniques must be considered to measure transverse properties and understand fundamental behavior in the transverse plane. The diametral compression test (also known as the Brazilian disk test) has been used to measure the hardness and strength of pharmaceutical pills [6], the splitting tensile strength of rock core and concrete specimens [7–9], and the apparent tensile strength of brittle materials that cannot be machined into conventional dog bone specimens [10]. Because of the simplicity of the test setup, the diametral compression test has also been used to measure transverse properties of oriented polymeric fibers [11]. Some studies have shown that flattening the ends of brittle cylindrical disks increased transverse tensile strength values by altering the modes of failure [12].

The analysis of a cylinder exposed to a concentrated line force applied at opposite sides is a classical problem for verification of theoretical and experimental methods to determine the exact state of stress or strain in a structural member [13]. The objective of this study is to understand the transverse material response of two pultruded composite rods subject to diametral compression loading. Diametral compression tests were conducted and the material response was observed and analyzed using acoustic emission (AE), digital image correlation (DIC), and finite element analysis (FEA).

* Corresponding author. Tel.: +1 213 740 1634.
E-mail address: nkar@usc.edu (N.K. Kar).
[1] Present address: Ajou University, San 5, Woncheon-dong, Yeongtong-gu, Suwon 443-749, Republic of Korea.

0266-3538/$ - see front matter © 2012 Elsevier Ltd. All rights reserved.
http://dx.doi.org/10.1016/j.compscitech.2012.05.001

The mode of failure in the plane was determined by *in situ* SEM investigations.

2. Experimental procedure

2.1. Materials

Two types of unidirectional composite rods were acquired for diametral compression testing (Composite Technology Corporation, Irvine, CA). The rods consisted of unidirectional carbon (CF) or glass fibers (GF) in an epoxy matrix (proprietary). The two composite rods featured the same epoxy and fibers used for the core (CF) and shell (GF) of the hybrid composite rod in CRCs. The all-carbon and all-glass rods (7 mm diameter) were produced by pultrusion, and are shown in Fig. 1. The fiber volume fraction was ~70% in both rods, with fiber diameters of ~8 μm (CF) and ~25 μm (GF). Test specimens were cut to a length of 152 mm, the length of compression platens used in the experiment.

2.2. Diametral compression and digital image correlation

A mechanical testing machine (Instron 5585) was used to apply diametral compression to the samples at a loading rate of 0.1 mm/min. The acoustic emission (AE) technique was employed during the tests to detect signals associated with damage. A single acoustic emission resonance transducer (300 kHz Micro 30, Physical Acoustics PCI-2) was placed on each rod to detect acoustic emission activity. Additionally, as each composite rod was compressed, a microscope was used to record images during loading to determine true displacements at the cylinder edges, as shown in Fig. 2a.

Digital image correlation (DIC) is a non-contact strain measurement technique that is used to measure non-uniform full-field displacements. To measure in-plane strains, white and black paint were sprayed in succession onto the rod surface to produce a random speckle pattern, as shown in Fig. 2b. The vertical displacements shown in Fig. 2c were determined by direct DIC measurements provided inputs for an analytical solution and a finite element model. Two-dimensional DIC was performed using commercial software (VIC-2D, Correlated Solution, Inc.).

2.3. Finite element analysis

Finite element analysis was performed to simulate the load–displacement response and strain distribution during diametral compression tests. A 3D, transversely isotropic, linear elastic model was developed using measured transverse properties (E_T, G_{xy}, v_{yx}), determined experimentally. The specimens were modeled to represent the geometrical features of the test setup using exact dimensions from the experiment. Load and boundary conditions were simulated with FEA software (ABAQUS) using 50,160 elements and a general-purpose brick element (C3D8R). The analysis involved a single step, in which a vertical displacement (determined via DIC) was applied using an analytically rigid surface and the reaction load was obtained.

2.4. Determination of transverse modulus

Jawad and Ward [14] developed a relationship for transversely isotropic materials from elasticity theory, relating the apparent transverse modulus (E_T) to the vertical displacement (u_y), load (F), length (L) and radius (R) for a diametral compression test:

$$u_y = \frac{4F}{\pi L E_T}\left(0.19 + \sinh^{-1}\left(\sqrt{\frac{\pi R E_T L}{4F}}\right)\right) \quad (1)$$

Eq. (1) is valid when the contact area under the loading platens is much less than the diameter of the cylinder, and has been used to determine transverse modulus values for continuous fibers [11], and was used to determine the transverse modulus of the composite rods from experimentally determined load and vertical displacement values.

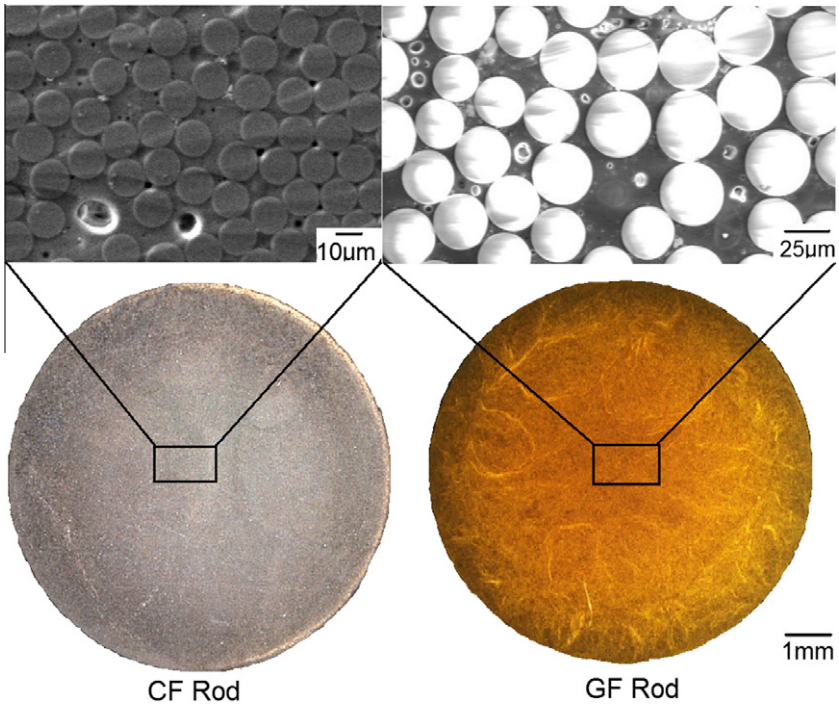

Fig. 1. Pultruded carbon fiber and glass fiber rods with common matrix.

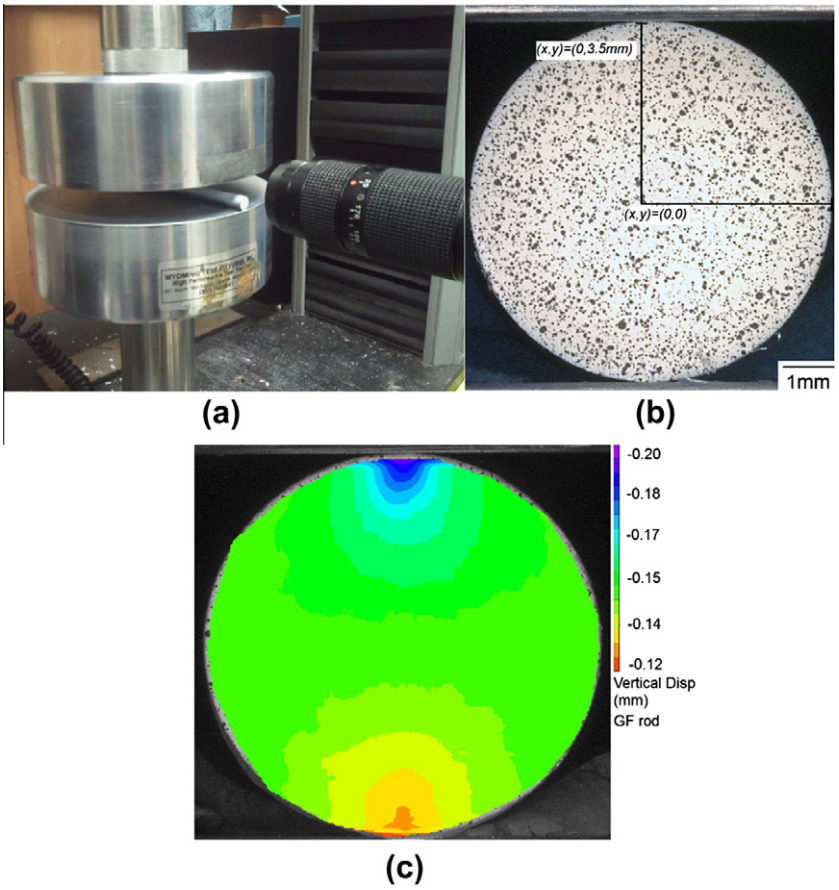

Fig. 2. (a) Keyence microscope and Instron used for DIC, (b) cross section of composite rod showing black and white random speckle pattern, and (c) displacement of GF rod at 33 kN.

3. Experimental results

3.1. Transverse behavior

The in-plane behavior and apparent transverse modulus (E_T) of each CF and GF composite rod were determined from diametral displacement(s) and corresponding load(s). Fig. 3a shows typical load- crosshead displacement curves for both composite rods and the amplitude decibel (dB) output for each detected AE hit. Correlation of AE amplitude distributions with different failure modes has been reported previously [15]. In many cases, authors use the AE amplitude distribution to identify specific damage mechanisms [15]. The initial, non-linear concave inflection of the curve is characteristic of Hertzian contact behavior [14]. The first burst of AE emission shown in the figure corresponds to this initial contact region. After this inflection, the load response was approximately linear up to failure, at which point the load dropped and a diametral crack appeared within the plane in both composite rods. Clusters of AE activity were apparent, showing detection in a dB output range of 30–60 dB, and final failure producing an output of 80–95 dB, corresponding to the diametral crack and the load drop. The increase in AE emission behavior before the load drop was an indication that damage mechanisms were active because the increase in the number of AE events is usually associated with increased damage [15]. However, it is incorrect to assume that the all the detected AE hits correspond to active damage mechanisms. The peak frequencies of the detected AE hits were also determined, and it was found that the initial peak frequencies for both rods up to the concave inflection point (at lower loads) were low, between 30 and 90 kHz. A typical waveform of a detected AE hit before final failure is also shown at the top of Fig. 3a. The waveform of the indicated hit before final failure shows a decibel output of 48 dB with a peak frequency of 173 kHz. Fig. 3b shows the maximum frequency distribution for the detected AE hits after Hertzian contact (post inflection point) and before the final failure AE burst. The majority of these detected peak frequencies for both composite rods were between 120 and 240 kHz, a frequency range which has been shown to be associated with matrix cracking in polymer composites [16]. Fig. 2c shows a vertical displacement field (measured by DIC) at ~33 kN for the GF composite rod. The measured DIC surface displacements in the figure show that the top and bottom regions of each composite surface were displaced downward because of vertical motion of both platens under the imposed load. The true displacement (u_{true}) is the difference between the displacement from the top (u_{top}) and bottom (u_{bottom}) regions of the composite surface, ($u_{true} = u_{top} - u_{bottom}$). The true displacement (u_{true}) was determined from successive images recorded at incremental loads.

The load vs. true displacement (u_{true}) curve is shown in Fig. 4a and b for both the CF and GF composite rods, indicating different behavior than shown in Fig. 3. The curves show three stages of deformation. Stage I represents the initial Hertzian contact region, while Stage II represents a linear elastic response of each rod. As both composites deformed in compression, a displacement and load were reached where inelastic behavior was apparent. The deviation from linearity was not observable in the load–displacement curves of Fig. 3, but was consistent with AE data which indicated active damage mechanisms. The reduction in slope shown in Fig. 4a and b reflects this behavior and is denoted as Stage III. While

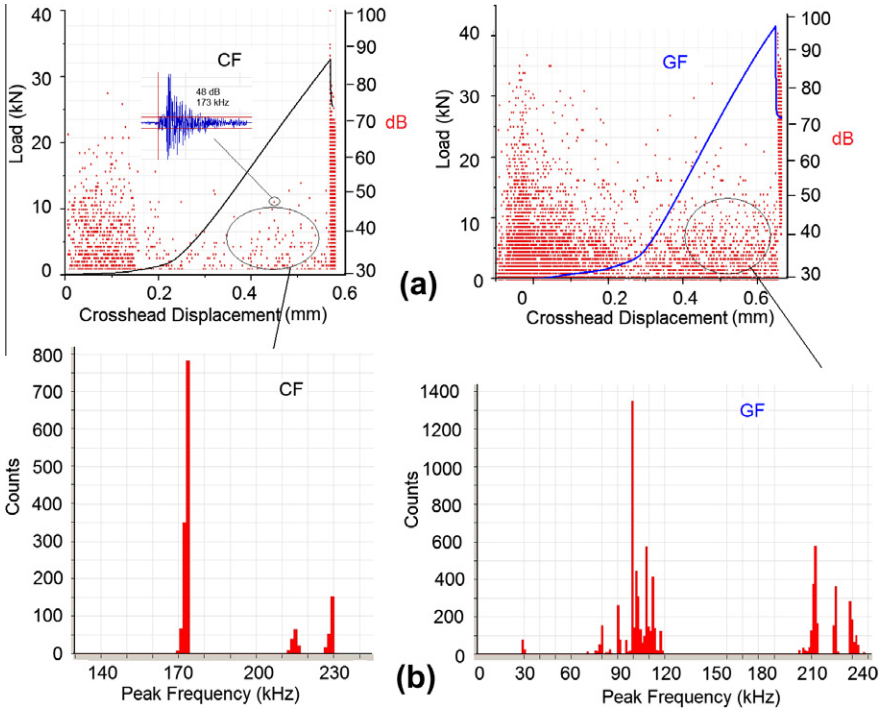

Fig. 3. (a) Typical load vs. crosshead displacement curves for the CF (left) and GF rods. (b) Typical peak frequency distribution for each CF and GF rod.

the composite rods continued to deform, the reduction was permanent, although both rods continued to support higher loads up to the point of failure.

Eq. (1) was solved numerically for E_T by inputting an experimental load value, assuming an initial value for E_T, and comparing the analytical displacement (u_y) with the true displacement (u_{true}) at the given load. Iterations were performed to minimize error in the value of E_T and promote convergence between the analytical and true displacements. Thus, the value of E_T was adjusted so that u_y equaled u_{true} for a specific load, shown in Fig. 4a and b as the analytical solution data.

The adjustment of the apparent transverse modulus for both the CF and GF rods as a function of true displacement is shown in Fig. 4c. Both curves show an increase in E_T for Stage I, with a peak and plateau in Stage II. The steady state value of E_T occurs in Stage II, where the CF and GF rods had average values of 10.78 ± 0.26 GPa and 12.8 ± 0.48 GPa respectively. While Eq. (1) is appropriate for determining elastic constants only in the linear elastic region (Stage II), values were determined for Stage III to quantify the effect of localized damage on bulk transverse properties, as shown in Fig. 4c. During Stage III, E_T decreased for both the CF and GF rods, but the CF rod showed a greater loss in apparent modulus compared to the GF rod (~25% vs. ~15% loss) at the end of Stage III (before final failure). Thus, damage mechanisms caused a reduction in the load–displacement response, with greater deformation and softening occurring in the CF rod. The transverse behavior of a composite is typically matrix dependent, but the fiber type and fiber architecture also contribute to the strength and modulus values. The GF rod showed a slightly greater apparent transverse modulus than the CF rod with equivalent fiber volume fraction and matrix. Studies have shown that E_T increases with an increasing E_f:E_m ratio, and E_T also shows a greater dependence at a higher V_f, where subscripts f and m are fiber and matrix, respectively [17]. The glass fiber is isotropic, with equivalent longitudinal and transverse properties that are ~6× greater than the transverse modulus of the transversely-isotropic carbon–fiber, which contributes to the observed greater E_T value for the GF rod.

The load–displacement behavior for diametral compression was simulated using a linear FE model. The transverse property inputs used were the average values of E_T from Stage II (10.78 and 12.8 GPa for the CF and GF respectively) for both composite rods as determined from Eq. (2), and longitudinal properties were used from a previous paper (5). The load–displacement curves for the FE simulation for each composite rod are also shown in Fig. 4a and b, and simulated curves match the measured curves within 5% in the linear elastic region (Stage II). The agreement between the experimental and simulation results during Stage II indicate that the diametral compression test is a suitable method for determining the transverse modulus of pultruded composite rods. The experiments show deviations from linearity for both composite rods in Stage III. This bifurcation from linearity was more pronounced in the CF rod, as the GF rod behaved linearly for a greater portion of the curve.

4. Analytical and computational results

4.1. Localized strain development

During diametral compression, a contact zone developed near the platen edges where the applied load became distributed over a finite region on the composite surface [18], which led to the development of in-plane shear and compressive strains. Fig. 5a shows the development of compressive (ε_y) and shear strains (γ_{xy}) near the loading edges from DIC and FE simulation for the CF composite rod at ~17 kN (Stage II). The shear strains arise on either side of the diametral line, but are zero along the line ($x = 0$), and axial-symmetry exists in both DIC and FE contours. The shear stress state at any point within a cylinder under diametral compression can be determined from [19,20]:

$$\tau_{xy} = \frac{2P}{\pi L}\left\{\frac{x(R-y)^2}{[x^2+(R-y)^2]^2} - \frac{x(R+y)^2}{[x^2+(R+y)^2]^2}\right\} \quad (2)$$

The shear stress for a given load in the linear elastic Stage II region was determined for both composite rods using Eq. (2). The (x,y) coordinates and the measured DIC shear strains (on either

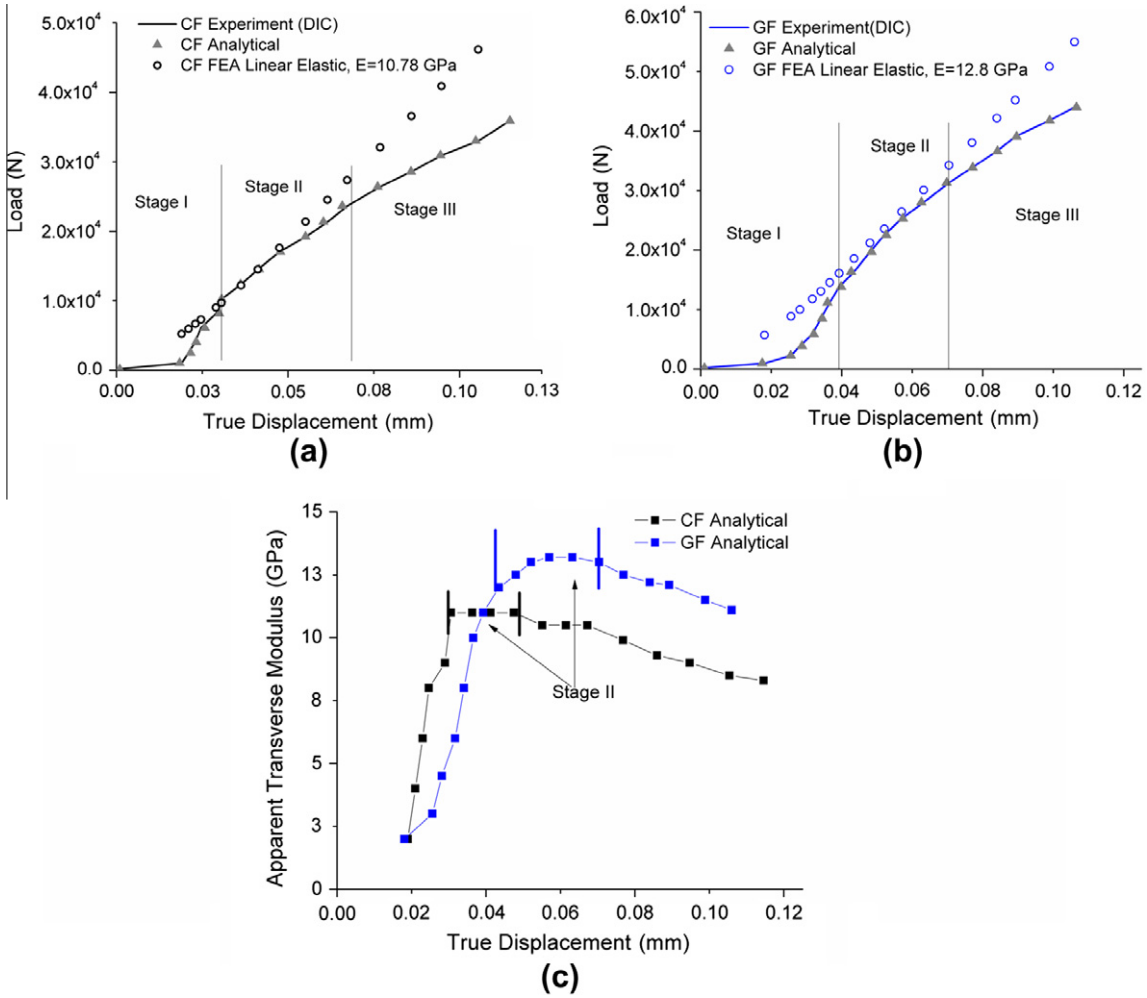

Fig. 4. (a) Load vs. true displacement curve for CF rod, (b) Load vs. true displacement curve for GF rod, and (c) variation of apparent transverse modulus as a function of true displacement.

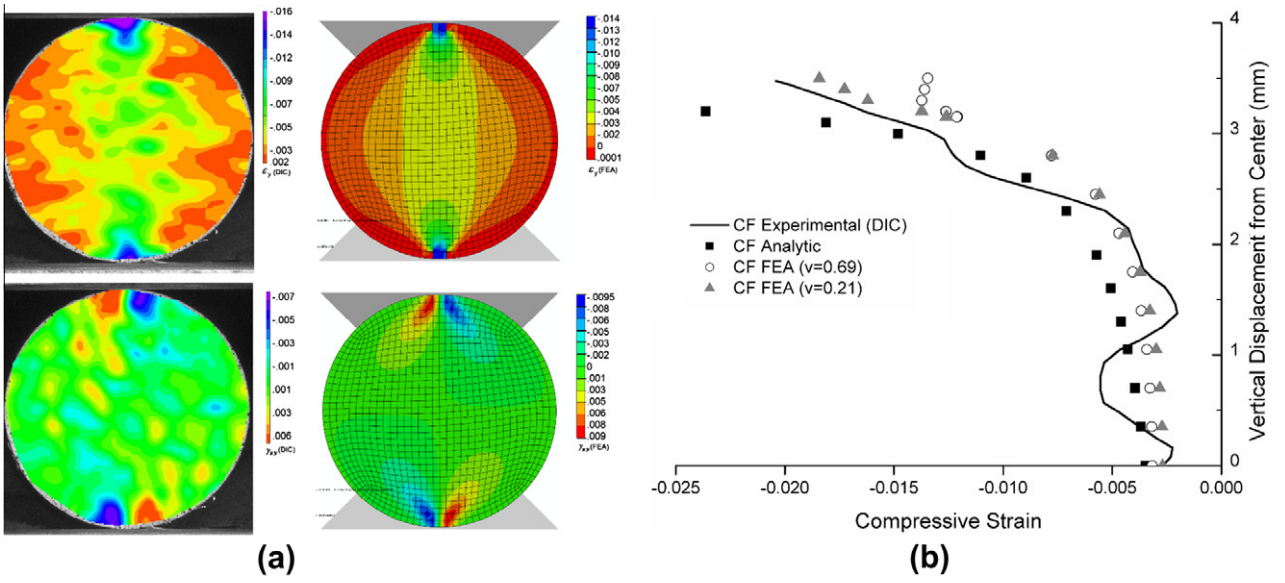

Fig. 5. (a) Compressive and shear strain contours of CF rod from DIC (left) and FEA analysis (right) under 17 kN. (b) Compressive strain distribution along diameter line of CF rod at 17 kN.

side of the diametral line-see Fig. 5) at each load value were determined from the contour maps via DIC. The analytical shear stresses and experimentally measured shear strains at specific loads (in Stage II) were used in combination with Hooke's law $\left(G_{xy} = \frac{\tau_{xy}}{\gamma_{xy}}\right)$

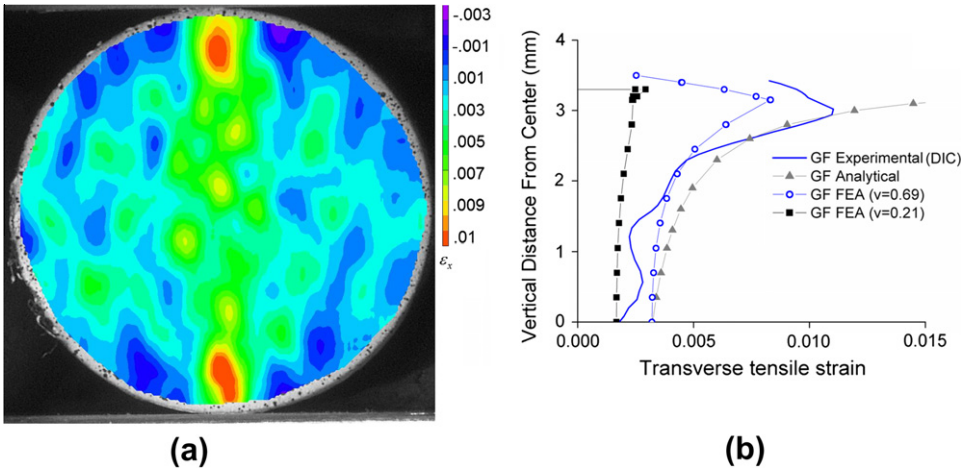

Fig. 6. (a) Transverse tensile strain contours from DIC for GF rod at 23 kN and (b) transverse tensile strain distribution along diameter line for GF rod.

to determine the in plane shear modulus. The values of the in plane shear modulus (G_{xy}) were 5.65 ± 1.05 GPa and 6.5 ± 0.96 GPa for the CF and GF rod, respectively and these values were used as transverse property inputs in the FE model.

The development of transverse tensile (ε_x) and compressive strains can also be determined analytically. The transverse tensile stress (σ_x) and compressive stress (σ_y) in the plane of a cylinder (with a diameter, D) under diametral compression are independent of material properties and orientation [15], and have been solved by Hertz with the following distribution along the diametral line ($x = 0$):

$$\sigma_x = \frac{2F}{\pi DL}, \quad \sigma_y = \frac{-2F}{\pi DL} - \frac{2F}{\pi L}\left[\frac{1}{R-y}\right] \tag{3}$$

Although this solution is for a point load, it is appropriate within the transverse plane. However, disagreement occurs near the rigid boundary contact point, [10] where analytical solutions are invalid. The stress field formed within the plane is the same for either plane stress or plane strain conditions [18]. The analytical expressions show that the transverse tensile stress σ_x is maximum and constant along the diametral line ($x = 0$), while at the center of the cylinder ($y = 0$), the compressive stress (parallel to the load direction) is equal to $-3\sigma_x$ and increases towards either loading edge. To determine the corresponding analytical strains, Hooke's law was used with a transverse Poisson's ratio $\left(\upsilon_{yx} = -\frac{\varepsilon_x}{\varepsilon_y}\right)$. The Poisson's ratio used for the FE model was ~0.69 for both composite rods. However, significant variation was evident, with values ranging from 0.40 to 0.69 for both the CF and GF rods determined at various loads (in Stage II) and was markedly higher from typical values of 0.21–0.28 [5]. Under pure transverse compression tests, the initial Poisson's ratio was 0.3–0.4, and with increasing load this value reached 0.6–0.7, due to micromechanical behavior including debonding between fiber and matrix. There have also been reports of Poisson's ratio values equal to 0.66 for unidirectional composites with high volume fraction of fibers [26].

The FE simulations were performed using measured transverse properties (E_T, G_{xy}, ν_{yx}), and Fig. 5b shows the compressive strain distribution along the diametral line ($x = 0$) up to the loading edge. Simulations were also performed at a lower transverse Poisson's ratio (see Fig. 5b). The strain distributions from DIC, FE ($\upsilon_{yx} = 0.21$ and 0.69), and analytical compressive strains at ~17 kN (Stage II) are shown for the CF rod. The results in Fig. 5b show that compressive strain was greatest just under the loading edges. The large compressive strains showed a weak dependence on the Poisson's ratio, as the compressive strain simulation for $\upsilon_{yx} = 0.21$ was similar to the simulation for $\upsilon_{yx} = 0.69$ along the diametral line.

The transverse tensile strain distribution determined from DIC at a load of 23 kN (Stage II) is shown in Fig. 6a for the GF composite rod. Fig. 6b shows the distribution of transverse tensile strains extending vertically from the center of the rod, approaching the rod edges for the DIC measurement, the FE simulation, and the analytical solution. The results show that the most intense transverse tensile strain occurs in a region ½ mm below the contact points. However, the tensile strains were roughly constant along the diametral line when a Poisson's ratio of 0.21 was used (under the same load). Tensile strain concentrations occurred in both composite rods under the loading edges as a result of localized debonding and microcracking. These cracks formed by transverse tension, caused by the high compressive strains under the loading edge, leading to a high $-\frac{\varepsilon_x}{\varepsilon_y}$ ratio measurement. The transverse Poisson's ratio input of 0.69 for the FE model characterizes this localized strain effect. The measured (DIC) and FE transverse strain distribution both show high strain values (~1%) in a localized region.

Fig. 7 shows the evolution of tensile strain (measured by DIC) in the CF rod as a function of applied load along the diametral line. At higher loads in Stage III, the tensile strain concentration increased

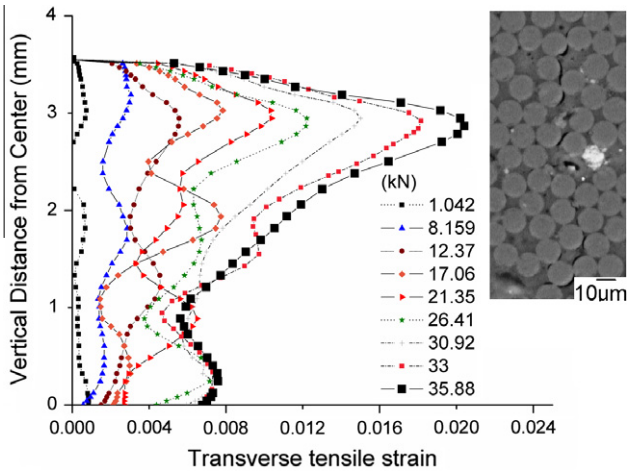

Fig. 7. Transverse tensile strain evolution in CF rod from DIC, formation of microscopic crack perpendicular to tensile strain direction in the strain concentration region.

significantly and became more localized under the platen edge, up to 2%. *In situ* SEM diametral compression tests were performed on CF samples to determine if and where damage mechanisms occurred during Stage III. Evidence of microcracking and debonding that led to the observed weakening in Stage III under the loading edges is shown in the SEM image. The localized ε_x strain concentrations were a result of the development of matrix microcracks along the fiber/matrix interface, extending perpendicular to the direction of the concentrated transverse tensile strain (parallel to the loading axis). These microscopic damage mechanisms coincided with the early AE activity shown in Fig. 3, and are consistent with studies indicating that lower amplitudes correspond with matrix cracking [21]. The onset of Stage III shown in Fig. 4 reflects the development of multiple matrix microcracks and high tensile strain concentrations in both composite rods. The top and bottom regions of the cylinder in Figs. 6 and 7 show the distribution of transverse tensile strain was localized, indicating that the bulk of the material in the plane continued to deform elastically (without microcracks) until final failure.

5. Discussion

The centers ($x = 0, y = 0$) of both composite rods were exposed to a biaxial stress state of transverse compression and transverse tension in the linear elastic region. It has been shown that the apparent transverse tensile strength (TTS) (using Eq. (3) and the load at failure) measured by diametral compression is expected to be approximately equal to the uniaxial transverse tensile strength of pultruded composite rods [22]. This assertion relies on the assumption that failure initiates from the rod center. For comparative purposes, the apparent TTS values (from an average of five samples) for the CF and GF composite rods were 21.62 ± 0.66 MPa, and 23.96 ± 0.85 MPa respectively. The transverse compressive stress is three times the tensile stress at the rod center, and increases significantly near the loading edges. These high transverse compressive stresses lead to transverse tensile strains, contributing to the formation of localized microcracking and debonding under the loading edges in the tensile direction. This form of tensile damage indicates that compressive stresses will reduce the nominal tensile stress to cause failure because of induced initial tensile strains. Thus, the apparent TTS can be a useful global indicator of relative transverse tensile strength among different composite rods (with different diameters and fiber types), but is a conservative estimate of TTS since the loading geometry forces a biaxial stress state, where the transverse compressive stress contributes to transverse tensile failure.

Microcrack coalescence led to a macroscopic crack along the diametral line (at the failure load) with a corresponding peak in AE activity, as shown in Fig. 8a for the GF rod and CF rod. Final failure was confined to the central region of the cylinder, and was brittle and catastrophic in nature; causing an instantaneous drop in load. Fig. 8b shows the deflection of the crack at an angle near the loading edges. Fig. 5a and b shows that both shear and compressive strains develop on either side of the diametral line, and this corresponded to the region where crack deflection occurred. The initial microcracking in the composite rods was governed by the principal direction of tensile strain, and final failure occurred along the diametral line where tensile stresses and strains were the highest. Since this was the only form of localized damage occurring before final failure, the orientation of the shear fracture planes depended on the shear (τ) and normal (σ) tractions, (obtained from the components of the stress tensor at failure) and fracture angle at a specific point, as discussed in [23]. Since the fracture angle was no longer perpendicular to the tensile direction, the fracture criteria changed, and showed similar failure angles produced by pure transverse compression [24]. Crack angles under transverse compression can be greater than 45° because failure occurs on a plane where the shear traction (τ) reaches a critical value that is dependent on the normal compressive traction (σ) based on the Mohr–Coulomb criteria [24,25]. Thus, mixed mode final fracture was observed, showing both matrix failure by tension along the diameter and shear failure due to dominant compressive and shear traction near the loading edges.

Fig. 8b shows the fracture surfaces of the GF and CF rod in the longitudinal direction. The CF surface reveals bare fibers with little

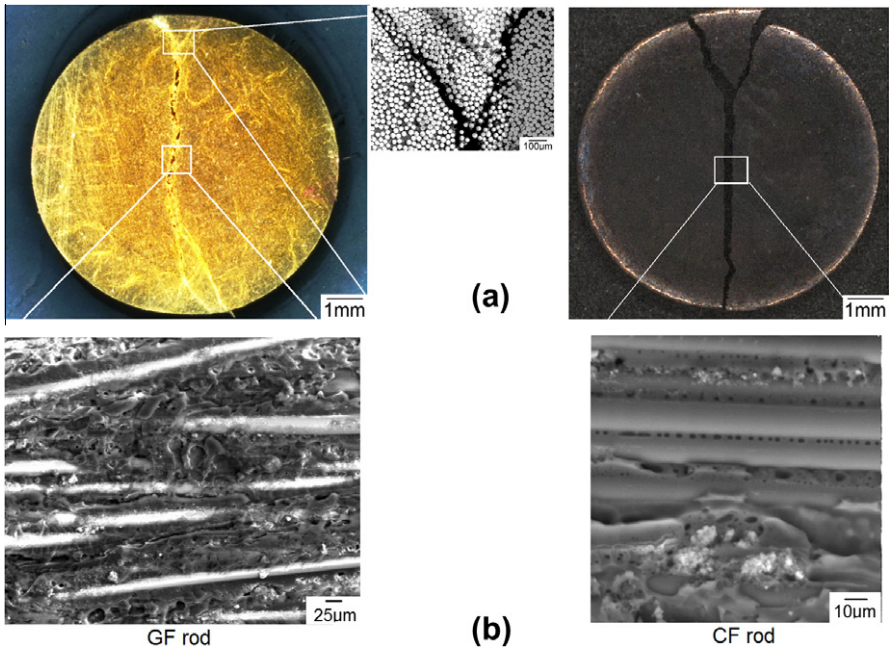

Fig. 8. (a) Diametral crack in GF and CF rod at failure with angled fracture near loading edges. (b) Fracture morphology showing bare CF fibers and residual glass fiber/matrix adhesion.

residual matrix attached, and regions of pure matrix with no fibers, indicating complete fiber–matrix separation. The GF fracture surface shows some residual adhesion of matrix to fibers, and some fibers embedded in the matrix. The fiber–matrix bond strength strongly affected the transverse behavior of the composite rods. The fracture surfaces indicated that the fiber/matrix bond in the CF rod was more prone to separation under transverse conditions when compared to the GF rod, and this was reflected in lower transverse modulus, strength values, and fractography. The mechanisms of interfacial bond strength depend primarily on the chemical bond and reactivity between fiber and matrix. Sizing coupling agents are applied to fiber surfaces as a means to provide a chemical link between the fiber and matrix, where co-reactivity of the sizing agent with both the fiber and matrix through covalent bonds produces molecular continuity [26]. The mechanisms of interfacial bonding of carbon fibers and polymer matrices have complications primarily caused by the high reactivity and absorbing nature of the carbon fiber surface [27]. However, such coupling agents used on the fibers in this study are proprietary, so the exact chemical cause for the higher degree of adhesion in the GF composite rod over the CF composite rod is speculative, and requires analysis that is beyond the scope of this work.

6. Conclusions

Diametral compression tests were performed on CF and GF pultruded composite rods to determine the effect of transverse loads on in-plane behavior and the GF composite showed greater resistance to transverse deformations and fracture than the CF rod. DIC was used to capture displacement and strain, and inelastic behavior was observed through changes in the load–displacement curve. The distribution of strains in the transverse plane of the composite rod showed a region of localized tensile strains under the loading edges which resulted from the formation of matrix microcracks and debonding. These cracks caused a reduction in load-bearing capability of both rods. Final failure occurred along the diameter, as a crack formed parallel to the direction of applied load, with shear failure near the loading edges.

While service loads will produce stress and strain conditions more complex than those considered here, the results provide insights into basic transverse behavior and development of associated damage mechanisms. The diametral compression test combined with DIC provides a means to directly measure transverse and in plane shear modulus, while in previous studies, an adapted Eshelby model was used to provide estimates of these properties [28,29]. Although approximations of material properties are often useful to provide engineering estimates, accurate property measurements in both the transverse and longitudinal directions are preferable for predictive modeling of component durability and lifetime. The deformations produced in this study were relatively simple, but yielded combined fracture modes, an indication of the complexity of composite fracture mechanics.

The findings presented here have implications for the intended application of such rods in overhead conductors (CRCs), which generally feature a GF shell around a CF core. The primary purpose of the GF shell of the rods is to prevent galvanic coupling between the CF core and the over-wrapped Al wires [4]. Attaching the conductors to lattice towers requires collet fixtures that grip the composite rods. In doing so, the collets introduce contact and transverse loads that include simple diametral compression, but generally are more complex. The well-documented susceptibility of unidirectional composites to surface wear and transverse crack damage may dictate measures to mitigate stress concentrations, or consider alternative fiber architectures to provide greater resistance to surface damage from localized stresses resulting from such grips.

Acknowledgments

The authors would like to thank Composite Technology Corporation for providing composite samples and Christopher Fisher for his insight and assistance.

References

[1] Kar NK, Barjasteh E, Hu Y, Nutt SR. Bending fatigue of hybrid composite rods. Composites: Part A 2011;42(3):328–36.
[2] Barjasteh E, Bosze EJ, Nutt SR. Thermal aging of fiberglass/carbon–fiber hybrid composites. Composites: A 2009;40(12):2038–45.
[3] Tsai YI, Bosze EJ, Barjasteh E, Nutt SR. Influence of hygrothermal environment on thermal and mechanical properties of carbon fiber/fiber glass composites. Compos Sci Technol 2009;69(3–4):432–7.
[4] Bosze EJ, Alawar A, Bertschger O, Tsai YI, Nutt SR. High-temperature strength and storage modulus in unidirectional hybrid composites. Compos Sci Technol 2006;66(13):1963–9.
[5] Kar NK, Hu Y, Barjasteh E, Nutt SR. Tension fatigue of hybrid composite rods. Composites: Part B 2012;43:2115–24.
[6] Cartensen JT. Pharmaceutics of solids and solid dosage forms. New York: John Whiley and Sons; 1977.
[7] Standard test method for splitting tensile strength of intact rock core specimens. ASTM D3967-86. 10. p. 504–6.
[8] Mellor M, Hawkes I. Measurement of tensile strength by diametral compression of discs and annuli. Eng Geol 1971;5(3):173–225.
[9] Hudson JA, Brown ET, Rummel F. The controlled failure of rock discs and rings loaded in diametral compression. Int J Rock Mech Min Technol 1972;9:241–8.
[10] Procopio AT, Zavaliangos A, Cunningham JC. Analysis of the diametrical compression test and the applicability to plastically deforming materials. J Mater Sci 2003;38(17):3629–39.
[11] Singletary J, Davis H, Song Y, Ramasubramanian MK, Knoff W. The transverse compression of PPTA fibers. J Mater Sci 2000;35(3):583–92.
[12] Fahad MK. Stresses and failure in the diametral compression test. J Mater Sci 1996;31(14):3723–9.
[13] Tokovyy YV, Hung KM, Ma CC. Determination of stresses and displacements in a thin annular disk subjected to diametral compression. J Math Sci 2010;165(3):342–54.
[14] Jawad SA, Ward IM. The transverse compression of oriented nylon and polyethylene extrudates. J Mater Sci 1978;13(7):1381–7.
[15] Barré S, Benzeggagh ML. On the use of acoustic emission to investigate damage mechanisms in glass–fibre reinforced polypropylene. Compos Sci Technol 1994;52:369–76.
[16] de Groot PJ, Wijnen PAM, Janssen BF. Real time frequency determination of acoustic emission for different fracture mechanisms in carbon/epoxy composites. Compos Sci Technol 1995;55:405–12.
[17] Kaw AK. Mechanics of composite materials. 2nd ed. CRC Press; 2006. p. 223–4.
[18] Liu C, Lovato ML. Elastic constants determination and deformation observation using Brazilian disk geometry. In: Proceedings of the XIth International Congress and Exposition. Society for Experimental Mechanics; 2008.
[19] Timoshenko SP, Goodier JN. Theory of elasticity. New York: McGraw-Hill; 1970.
[20] Frocht MM. Photoelasticity. New York: John Wiley and Sons; 1947.
[21] Berthelot JM, Rhazi J. Acoustic emission in carbon fibre composites. Compos Sci Technol 1990;37:411–28.
[22] Chisholm JM, Hahn HT, Williams JG. Diametral compression of pultruded composite rods as a quality control test. Composites 1989;20(6):553–8.
[23] Pinho ST, Iannucci L, Robinson P. Physically-based failure models and criteria for laminated fibre-reinforced composites with emphasis on fibre kinking. Part I: Development. Composites: Part A 2006;37(1):63–73.
[24] Gonzalez C, LLorca J. Mechanical behavior of unidirectional fiber-reinforced polymers under transverse compression: microscopic mechanisms and modeling. Compos Sci Technol 2007;67(13):2795–806.
[25] Collings TA. Transverse compressive behaviour of unidirectional carbon fibre reinforced plastics. Composites 1974;5(3):108–16.
[26] Koenig JL, Emadipour H. Mechanical characterization of the interfacial strength of glass reinforced composites. Polym Compos 1985;6:142–50.
[27] Kim JK, Mai YW. Engineered interfaces in fiber reinforced composites. Elsevier Science; 1998. p. 170–80.
[28] Burks BM. Short-term failure analysis of aluminum conducting composite core transmission lines. Master's Thesis, University of Denver; 2009.
[29] Burks B, Armentrout D, Kumosa M. Characterization of the fatigue properties of a hybrid composite utilized in high voltage electric transmission. Composites: Part A 2011;42:1138–47.